Available online at www.sciencedirect.com

ScienceDirect

Energy Procedia 38 (2013) 582 – 588

Energy Procedia

SiliconPV: March 25-27, 2013, Hamelin, Germany

Interaction of iron with extended defects in multicrystalline silicon studied by local gettering

Patricia Krenckel[a], Philipp Saring[a], Marie A. Falkenberg[a], Vitaly Kveder[b], and Michael Seibt[a]

[a]*IV. Physikalisches Institut, Georg-August-Universität Göttingen, Friedrich-Hund-Platz 1, 37077 Göttingen, Germany*
[b] *permanent address: Institute of Solid State Physics, Russian Academy of Science, 142432 Chernogolovka, Russia*

Abstract

In order to adjust temperature treatments during solar cell processing to multicrystalline silicon, the interactions of metal impurities in multicrystalline silicon with extended defects like grain boundaries have to be understood. For this purpose, we investigate neighboring wafers of block-cast multicrystalline silicon intentionally doped with iron during crystal growth. Samples are investigated with LBIC after aluminum gettering (AlG) experiments with an Al layer only on parts of the sample at different temperatures. LBIC data are quantitatively analyzed using two-dimensional gettering simulations and pattern recognition techniques combined with multivariate statistics. LBIC-images and simulations show pronounced regions of reduced excess carrier recombination around grain boundaries (denuded zone) in uncovered regions. This can be attributed to impurity accumulation at grain boundaries and their related depletion in the adjacent bulk. In covered regions, no denuded zones are observed. Temperature variation provides evidence that our experiments are mainly in the regime where gettering efficiency is limited by impurity precipitate dissolution, unless the temperature is chosen well above the solubility temperature corresponding to the average iron concentration.

Selection and/or peer-review under responsibility of the scientific committee of the SiliconPV 2013 conference

Keywords: multicrystalline silicon; impurity interaction; iron contamination; grain boundaries; denuded zones; aluminum gettering; LBIC; simulations

1. Introduction

Block-cast multicrystalline silicon is a low-cost standard material for solar cells. However, its potential is limited by a rather high contamination level of impurities [1] originating from the feedstock, crystal growth environment and also wafer processing under non clean room conditions [2]. Iron is considered as one of the most detrimental metal impurities forming point defects on interstitial sites or as iron boron pairs, but also accumulating at structural defects due to segregation or precipitation. In either case they

1876-6102
Selection and/or peer-review under responsibility of the scientific committee of the SiliconPV 2013 conference
doi:10.1016/j.egypro.2013.07.320

are related to substantial decreases of the minority carrier diffusion length. To remove the impurities from active device regions, several gettering techniques have been developed, as reviewed in [3], among which AlG is a conceptually simple technique based on the segregation of impurities in a liquid Al:Si layer at the back surface. Due to the instantaneous formation of the Al:Si layer, mainly during heating to processing temperature [4], it provides a powerful tool to study the interaction of impurities with extended defects, their accumulation and dissolution there, and also precipitation.

Here, we use AlG to study iron distribution in multicrystalline silicon after crystal growth and gettering treatments at various temperatures and different cooling rates. We use an approach where a spatially confined Al layer allows directly separating effects of gettering, thermal annealing, and cooling. Two-dimensional gettering simulations are used to compare to quantitatively analyzed data extracted by pattern recognition techniques and multivariate statistics.

2. Experimental

In order to have similar grain structures, samples were taken from ~200μm thick wafers that had been cut from neighbouring regions of block-cast multicrystalline silicon grown from an intentionally iron contaminated melt. Samples were polished on one side, cleaned in water and organic solvents, and finally etched in $HF:HNO_3$. A 250nm aluminum layer was evaporated through a mask on the polished surface subsequent to a HF-dip. The resulting Al layer covered about one third of the sample backside. Gettering treatments were carried out in argon atmosphere at 900°C, 950°C, and 1025°C for 50min followed by a slow cooling with an approximate a rate of 0.05K/s. The semi-transparent aluminum front contact was prepared on the side which was not covered by aluminum during annealing. LBIC measurements were performed with a spatial resolution of 25μm under low injection conditions at wavelengths of 850nm and 760nm which allows determining the diffusion length.

3. Results

3.1 Observations

In the reference material (Fig. 1(a)), representing the as grown status, two types of grain boundaries can be distinguished. Some grain boundaries (I) reveal rather small LBIC-contrasts or, as many twin boundaries identified from additional defect etching, are invisible. On the other hand, several grain boundaries (II) with strong contrast are accompanied by an environment with increased signal indicating an impurity-denuded zone due to preferred agglomeration of impurities at these grain boundaries upon cooling, which can be understood in the context of structural arguments [5].

Large intragranular regions reveal diffusion lengths around 30μm whereas the small grains, in case of overlapping of the denuded zones, show slightly increased diffusion lengths. Additional defect etching revealed strongly inhomogeneous dislocation densities between $10^4 cm^{-2}$ and $10^6 cm^{-2}$ with sometimes noticeably higher dislocation densities in small grains.

Fig. 1(b) shows a neighbouring sample after AlG at 950°C and slow cooling. Significant changes of the diffusion length can be observed, i.e. a decreased diffusion length in regions outside the influence of the Al:Si layer, after 950°C indicating partial dissolution of metal atoms from precipitates at grain boundaries and dislocations and their distribution in the bulk region. Below the gettering layer, the diffusion length progressively improves with increasing temperature from 900°C to 1025°C indicating that precipitate dissolution limits AlG kinetics rather than segregation in the Al:Si layer. After 1025°C, low recombination active structures such as twin boundaries can be resolved.

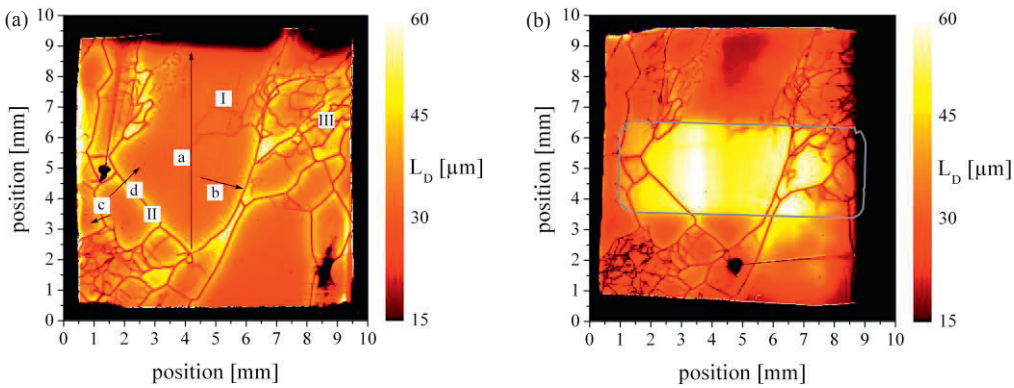

Fig. 1. Minority carrier diffusion length map (a) in the reference material. Grain boundaries with denuded zones (II) reveal by trend strong contrasts, whereas other grain boundaries (I) are nearly invisible. Small grains (III) reveal by trend larger diffusion lengths. After AlG at 950°C, depicted in (b), the diffusion length below the gettering layer (surrounded by gray line) has increased, elsewhere the diffusion length has decreased.

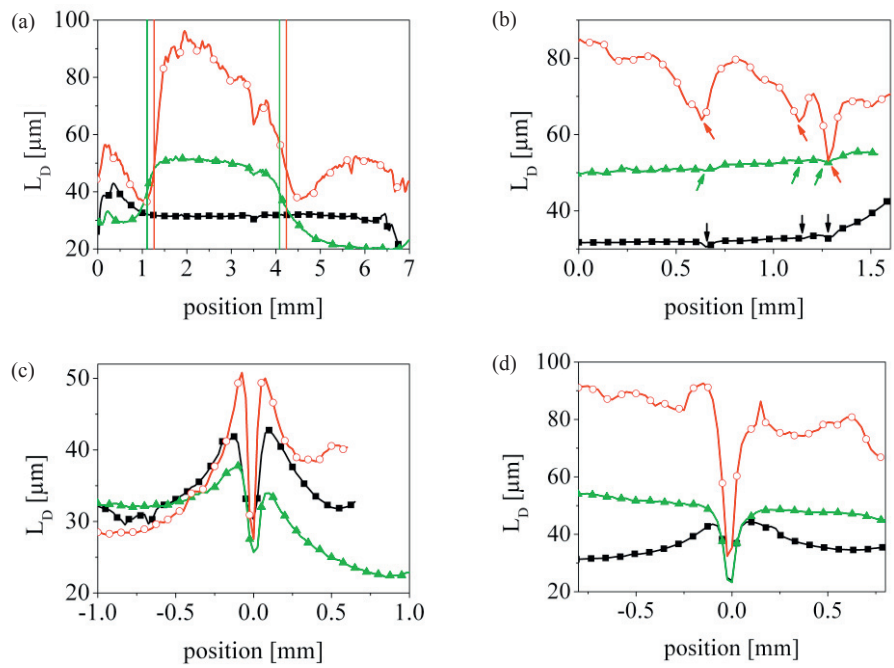

Fig. 2. Diffusion length profiles at positions indicated in Fig.1(a) for as grown (black squares), after 1025°C (red circles) and after 950°C (green triangles). (a) In the intragrain regions below the Al:Si layer (vertical lines), the diffusion length increases with AlG temperature, (b) revealing low recombination active structures such as twin grain boundaries. (c) At grain boundaries outside the influence of the gettering layer, denuded zones appear again after annealing, (d) whereas below the gettering layer the diffusion length has increased above the level of the denuded zones.

For a more detailed phenomenological description, diffusion length profiles are shown in Fig. 2 obtained for the as grown material (black squares), after AlG at 950°C (green triangles) and AlG at 1025°C (red circles) from different regions. Profiles across the Al-covered region (Fig. 2(a)) show strong gettering for both AlG treatments, a slight decrease or increase of the diffusion length in uncovered regions for 950°C and 1025°C, respectively. Fig. 2(b) reveals the intersecting observation that some coherent Σ3 twin boundaries are virtually 'invisible' in as grown material and after AlG at 950°C, whereas a strong contrast is observed after 1025°C on a much higher diffusion length level. Figs. 2(c) and (d) compare the formation of denuded zones in uncovered regions (c) for all conditions. In Al covered regions denuded zone formation is never observed.

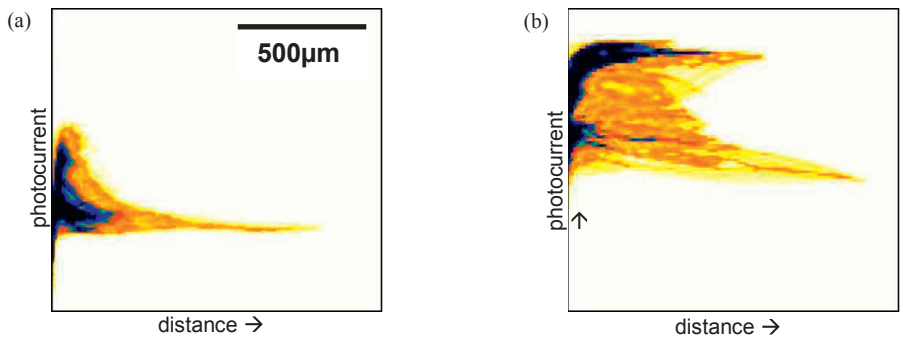

Fig.3. Two-dimensional relative frequency histograms of the LBIC signal ('photocurrent') versus distance to the next grain boundary. (a) as grown state; the distinct maximum for small distances reflects the formation of denuded zones while the lower value for large distances shows the small diffusion length in the center of large grains. (b) after AlG and slow cooling; two branches are observed belonging to regions with and without Al layer. Please note, that both graphs have identical scales.

In order to quantitatively compare experimental data between different AlG conditions and with 2D or 3D gettering simulations, a statistically meaningful data analysis is necessary. As a first step, we have implemented a simple pattern recognition technique to classify local LBIC data according to properties such as the distance to the next grain boundary. Fig. 3 shows typical results for the as grown state (left) and after AlG followed by slow cooling (right) in form of histograms. For the as grown state they clearly reveal the denuded zone around grain boundaries (high photocurrent at small distances) and the quite small photocurrent observed in large grains (branch at large distances). After AlG two branches are observed at large distances which correspond to regions with and without Al layer. In addition, the lack of denuded zones below the Al layer is seen by the monotonous increase of the LBIC signal with distance for the upper branch. It should be added that a more detailed classification is necessary to fully grasp the information content of LBIC maps.

3.2. Simulations

To simulate impurity redistribution (mainly iron) between bulk, grain boundary, and gettering regions during annealing and subsequent cooling, we have extended our simulation model [4] to two dimensions. For this purpose, we use a finite element method (FEM) implementation on the basis of the software environment of COMSOL Multiphysics package. The program solves the time-dependent diffusion equation for an impurity (here: iron in silicon) including a reaction term describing precipitate dissolution and growth in a mean-field approximation [4]. The grain boundary is modelled as a plane with a precipitate density exceeding that in the bulk. Boundary conditions are zero flux at free surfaces and a

concentration ratio according to the segregation coefficient measured in [6] at the interface between silicon and the aluminum layer, i.e. we assume local equilibrium there.

For comparison with LBIC data, the interstitial iron concentration is converted to diffusion length using the formula for Shockley-Read-Hall recombination [7] [8] using the data reported in [9]. Note that this approach completely neglects excess carrier recombination at precipitates and also other extended defects.

As the initial state, we simulated the as grown sample assuming a total initial concentration of interstitially dissolved iron of $5 \cdot 10^{13} cm^{-3}$. Nucleation site densities for iron silicide precipitates were adjusted to of $2 \cdot 10^{6} cm^{-3}$ in the bulk and $1 \cdot 10^{7} cm^{-2}$ at the grain boundary resulting in an iron distribution in accord with the observed diffusion lengths in as grown samples. The resulting concentration profiles of interstitial and precipitated iron served as an input for simulations of subsequent processing with or without AlG.

Two-dimensional gettering simulations reproduce the essential results of the experiments. Fig. 4 supports the observation that denuded zones appear for all temperatures (and slow cooling rates) in uncovered regions, i.e. without aluminum gettering.

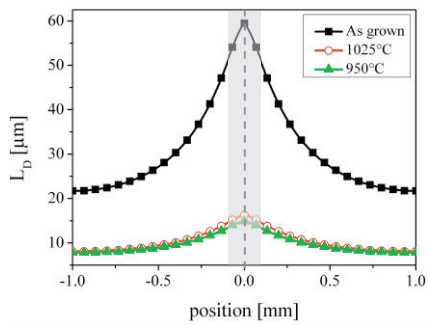

Fig. 4. Diffusion lengths calculated from simulated concentration profiles after different temperature treatments without aluminum gettering for a grain size of 2mm. The dashed line indicates the position of the grain boundary. It shows denuded zones adjacent to the grain boundary. Please note that the shaded region shows differences in comparison to measured profiles due to the simplified recombination model used.

It shows the diffusion length calculated from simulated concentration profiles across a grain boundary after different temperature treatments in the uncovered region for a grain size of 2mm. While the profiles for the as grown sample and for 950°C fit well with the experimentally determined diffusion length in Fig. 2(c), the profiles for 1025°C differ in relation to the profile for the as grown sample and in strength of the denuded zone. The region very close to the grain boundary (shaded) differs from the measured diffusion length profiles because the model does not take excess carrier recombination due to the grain boundary and its contamination into account.

A variation of grain size in the simulations of the uncovered region as shown in Fig. 5 illustrates a smaller diffusion length in larger grains due to less grain boundary accumulation of the impurity, i.e. less ‘cleaning’ of large grains during the cooling period of crystal growth.

The minimum diffusion length, i.e. the diffusion length within the grain at the largest distance from the grain boundary is shown for different grain sizes and different temperature treatments. All graphs show the same trend of remarkable smaller diffusion length for large grains as shown in Fig. 1(a) for the as grown sample. In contrast to the experiment, the samples at 1025°C and 950°C annealing show very similar diffusion length for all grain sizes in accord with the assumption of precipitates being the only sink and source of mobile impurities and the iron content of the material. This suggests additional effects

being important in the experiment for 1025°C which are not included in the simulations, e.g. surface gettering or immobile iron strongly bound to extended defects, as e.g. in dislocation cores.

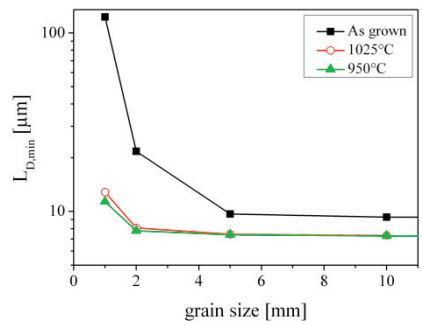

Fig. 5. Minimum diffusion length within the grain for different grain sizes. The different graphs show different temperature treatments. It can be seen that larger grains show lower diffusion lengths for all temperature treatments. In contrast to the experiment the samples with 1025°C and 950°C annealing show the same diffusion length which is lower than the as grown sample.

In Fig. 6, the diffusion length is shown versus distance from the grain boundary for different grain sizes of the as grown sample. The formation of denuded zones can be seen in accord with experimental data shown in Fig. 3(a). The gray dotted lines indicate further variation of the grain size which would lead to a comparable graph as Fig. 3(a). Fig. 6 contains additional information about the diffusion length for different grain sizes revealing the trend that small grains have higher diffusion length than large grains.

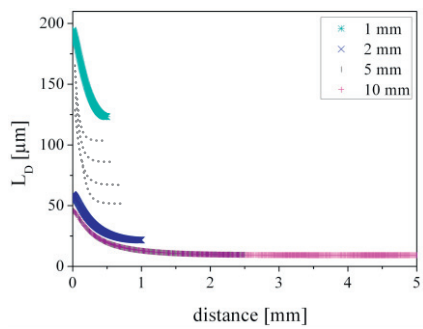

Fig. 6. Diffusion length versus distance from the grain boundary for the as grown sample for different grain sizes. The dotted lines imply the transition from simulations to measurements with many different grain sizes. The graph shows small diffusion length for large grains and the denuded zones comparable to Fig. 3(a). Additionally, it contains information about the grain size.

4. Conclusion

Local gettering procedure has been applied to multicrystalline silicon and investigated with LBIC. Pattern recognition and two dimensional simulations were used to quantitatively analyse the LBIC data.

Considerably different phenomena are observed below the Al:Si-layer and in uncovered regions. In the range of the gettering layer, the diffusion length is increased in comparison to the as grown material. Increasing diffusion lengths for temperatures even above the solubility temperature indicate that the gettering efficiency is limited by the dissolution of precipitates and presumably also by mobilization of strongly bound iron impurities at extended defects. In contrast to regions below the gettering layer,

uncovered regions show denuded zones adjacent to the grain boundaries and higher diffusion lengths for small grains due to impurity accumulation at the grain boundaries.

For better comparison of simulations with the experimentally determined diffusion length, we are currently including excess carrier recombination at the grain boundary into the simulation tool. Clearly, further investigations are necessary to reveal the origin of the discrepancy between simulation and LBIC measurements for annealing at high temperatures (1025°C) with the unexpected result of an overall improvement of the material even in areas remote from the Al gettering layer.

Pattern recognition analysis has shown that it is possible to transfer LBIC measurements into a more general context. However, as the results of the analysis not yet contains all information contained in experimental data, e.g. the information about grain sizes, this analysis has to be generalized and extended.

Acknowledgements

We gratefully acknowledge valuable support from B. Schlieper-Ludewig. This work was partly supported by the German Federal Minstry for the Environment, Nature Conservation and Nuclear Safety via research clusters SolarFocus (0327650 B) and SolarWinS (0327259 B) projects and the industry partners. The content of this publication is the responsibility of the authors.

References

[1] Buonassisi T, Istratov AA, Pickett MD, Heuer M, Kalejs JP, Hahn G et al. Chemical Natures and Distributions of Metal Impurities in Multicrystalline Silicon Materials. *Prog. Photovolt: Res. Appl* 2006;**14**;513-31.

[2] Riepe S, Reis I, Kwapil W, Falkenberg MA, Schön J, Behnken H. Research on efficiency limiting defects and defect engineering in silicon solar cells - results of the German research cluster SolarFocus. *phys. stat. sol. (c)* 2010;**8**;733-8.

[3] Seibt M, Kveder V.Gettering processesand the role of extended defects. In: Pizzini S, editor. *Advanced Silicon Materials for Photovoltaic Applications*, United Kingdom: John Wiley & Sons, Ltd.; 2012, p. 129-188

[4] Seibt M, Sattler A, Rudolf C, Voss O, Kveder V, Schröter W. Gettering in silicon photovoltaics: current state and future perspective. *phys. stat. sol. (a)* 2006;**203**;696-713.

[5] Chen B, Chen J, Sekiguchi T, Saito M, Kimoto K. Structural characterization and iron detection at Σ3 grain boundaries in multicrystalline silicon. *J. of Appl. Phys.* 2009;**105**;113502.

[6] Abdelbarey D, Kveder V, Schröter W, Seibt M. Aluminum gettering of iron in silicon as a problem of the ternary phase diagram. *Appl. Phys. Lett.* 2009;**94**;061912.

[7] Hall RN. Electron-Hole Recombination in Germanium. *Phys. Rev.* 1952;**87**;387-8.

[8] Shockley W, Read WT. Statistics of the Recombinations of Holes and Electrons. *Phys. Rev.* 1952;**87**;835-42.

[9] Istratov AA, Hielmair H, Weber ER. Iron contamination in silicon technology. *Appl. Phys. A* 2000;**70**;489-534